A Low-Order Dynamic Model for Planar Solid Oxide Fuel Cells Using Online Iterative Computation

Handa Xi

Jing Sun[1]
e-mail: jingsun@umich.edu

Department of Naval Architecture and Marine Engineering,
University of Michigan,
Ann Arbor, MI 48109

High-fidelity dynamic models of solid oxide fuel cells (SOFCs) capture the spatial distribution of key performance variables by considering the cells as distributed parameter systems. As such, they are often complex and require extensive computational resources. In this paper, driven by the need to support the control strategy development and system optimization, we develop a low-order SOFC model by approximating the mass and energy balance dynamics in the fuel and air bulk flows using quasi-static relations. However, due to the coupling between the quasi-static mass balance and current distribution, this approximation leads to a large set of coupled nonlinear algebraic equations that have to be solved online using iterative computation. In order to mitigate the computational cost involved, an efficient iterative algorithm is proposed to solve these equations. The new algorithm requires to iterate on only one variable—the cell voltage—to determine the current and flow compositions and their distributions. The low-order model with 16 states is compared to the baseline model, which has 160 states that incorporates fully the mass and energy balance dynamics. Simulations are performed to evaluate the model performance for both steady-state and transient operations, and to assess the computational cost associated with the low-order and full order models. It is shown that the low-order model closely matches the original baseline model, while the computation time is reduced by more than 50% compared to the baseline model.
[DOI: 10.1115/1.2931491]

1 Introduction

Solid oxide fuel cells (SOFCs) emerge as an attractive alternative energy solution for a wide range of applications, including stationary power plants and mobile auxiliary power units (APUs) [1]. Governments, universities, and industrial research laboratories around the world are investing significant resources in addressing material, manufacturing, and system integration issues associated with SOFC.

As the SOFC technology evolves rapidly, high-fidelity mathematical models that can predict the SOFC's dynamic characteristics become critical tools for the design, evaluation, and optimization of SOFC systems. Substantial progress has been made in the SOFC model development, and several dynamic models have been reported in recent years [2–8]. However, given the high complexity of SOFC, such as involved reaction kinetics, spatially distributed parameters, multiple species, and complicated heat transfer, high-fidelity models often require intensive computational resources, making them infeasible for system integration and control system development.

Meanwhile, transient operation issues such as slow load following and large overshoots of temperature and temperature gradient have been identified in the dynamic response of SOFC systems [8–11], necessitating the use of feedback control strategies to improve their transient performance. Systematic model-based control design and analysis that can leverage existing methodologies and toolboxes favor the use of low-order models, putting limitations on model complexity and computational demands. Therefore, a low-order model, which preserves the key dynamic characteristics of the system without imposing substantial computational demand, is in high demand to facilitate model-based control design and analysis.

It is noted that the SOFC is usually considered as a distributed parameter system, given the considerable spatial distributions of variables such as temperatures, pressures, and currents in the cell. Finite-volume method is often used to derive the dynamic model [4,7,8]. Using this approach, the total number of states in the SOFC model will be the product of the number of discretization units and the number of states in each of these units. In the model developed in Ref. [8], there are 12 states in each discretization unit, representing the concentrations of different species in the gas flows and the temperatures of different structure layers. Therefore, it is effective to reduce the number of states required in each unit to reduce the total number of states in the SOFC model.

In Refs. [2,5,12,13], the mass and energy balance dynamics in the fuel and air bulk flows are described by quasi-static relations, i.e., the dynamics are assumed sufficiently fast to reach their steady states instantaneously, given the high velocities of the bulk flows and the small channel volumes. Under this quasi-static assumption, all the governing Ordinary Differential Equations (ODEs) associated with the gas flow dynamics are replaced by algebraic equations, thereby eliminating all the states in these equations. The coupling between the mass balance and equipotential current distribution, however, results in a large set of coupled nonlinear algebraic equations, which have to be solved simultaneously using iterative algorithm. In this paper, we exploit the coupling relations between the unknown variables in these equations and propose an efficient online iterative algorithm to mitigate the computation intensity. For the proposed new algorithm, only one unknown variable, which is the cell voltage, needs to be iterated on to find the solution for the quasi-static mass balance and current distribution, leading to significant computation reduction.

[1]Corresponding author.
Manuscript received November 21, 2006; final manuscript received May 8, 2007; published online September 11, 2008. Review conducted by Umberto Desideri.

Copyright © 2008 by ASME

Downloaded From: http://fuelcellscience.asmedigitalcollection.asme.org/ on 03/19/2013 Terms of Use: http://asme.org/terms

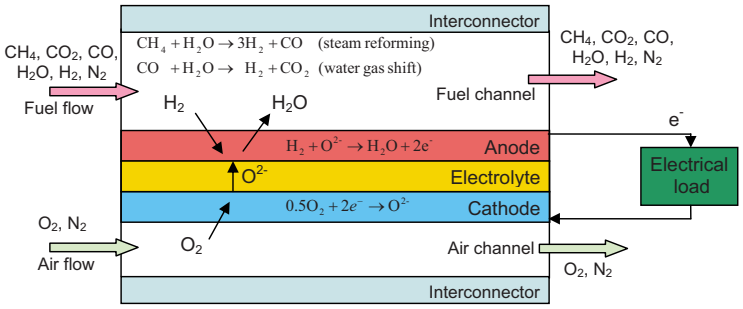

Fig. 1 Operating principle of co-flow planar SOFCs

In the remainder of this paper, a baseline model, which serves as a reference for the low-order model, is first described in Sec. 2 while the reduced-order model is derived in Sec. 3. In order to solve the coupled nonlinear algebraic equations resulting from the quasi-static mass balance and current distribution, an efficient online iterative algorithm is designed. These two models are then compared, through simulations, in Sec. 4 to establish the validity and to verify the computation efficiency of the simplified model, before drawing the conclusions in Sec. 5.

2 Baseline Model for Co-flow Planar SOFCs

A dynamic model for the co-flow planar SOFC is developed in this section, in order to establish a baseline for the subsequent model reduction effort. The operating principle of the SOFC considered in this paper is illustrated in Fig. 1. Different reforming approaches, such as the steam reforming (SR) and catalytic partial oxidation (CPOX), have been used to process the fuel before entering the fuel cell (i.e., prereforming), and they result in different compositions of the reformate fed into the SOFC. To make the SOFC model compatible with different system configurations, six species, namely, methane (CH_4), carbon monoxide (CO), carbon dioxide (CO_2), hydrogen (H_2), steam (H_2O), and nitrogen (N_2), are considered in the fuel flow. The fuel inlet to the SOFC can be any combinations of these six species. Dry air is fed into the cathode of the SOFC as the oxidant and coolant.

Direct internal reforming (DIR) is also included in the model developed in this paper. Because of the high operating temperature, the DIR is possible for the SOFC, allowing CH_4 to be reformed directly in the fuel channel through the SR and water gas shift (WGS) reactions [1]. DIR is beneficial in improving the system efficiency and reducing the size and cost of the external reformer [14]. Table 1 lists all the reactions to be considered in the SOFC model.

Table 1 Reactions considered in the model

Location	Reaction	Expression
Fuel channel	SR	$CH_4+H_2O \rightarrow CO+3H_2$
	WGS	$CO+H_2O \leftrightarrow CO_2+H_2$
Anode	Ox	$H_2+O^{2-} \rightarrow H_2O+2e^-$
Cathode	Red	$0.5O_2+2e^- \rightarrow O^{2-}$

To capture the spatial distribution of variables such as temperature, species concentration, and current density along the flow field, the finite-volume method [4,7,8,15] is applied in this paper to derive the model for the co-flow planar SOFC shown in Fig. 1. Using this approach, the cell is virtually divided into a user-defined number of units along the gas flow direction, as illustrated in Fig. 2, where the electrode and electrolyte layers are considered as one assembly structure, called positive electrode-electrolyte-negative (PEN) electrode. In one discretization unit, the variables such as the current density, temperatures, and pressures are assumed to be homogeneous. Dynamic governing equations for each unit in the SOFC model are derived by applying the electrochemical, thermal dynamic, and fluid flow principles. These discretization units are then integrated to form the SOFC model by imposing the gas flows, heat exchanges, and current distribution relations. The following assumptions are used in developing the model:

1. the cell is considered equipotential
2. the current is produced only by the oxidation of H_2, and CO only reacts through the WGS reaction
3. ideal gas flows for the bulk flows in both fuel and air channels
4. constant Nusselt number
5. adiabatic boundaries for the cell

In our model, each discretization unit has three submodels, namely, the electrochemical submodel, mass balance submodel, and energy balance submodel, which are summarized in Sec. 2.1–2.3.

2.1 Electrochemical Submodel. The operating voltage of one discretization unit of the cell can be calculated by

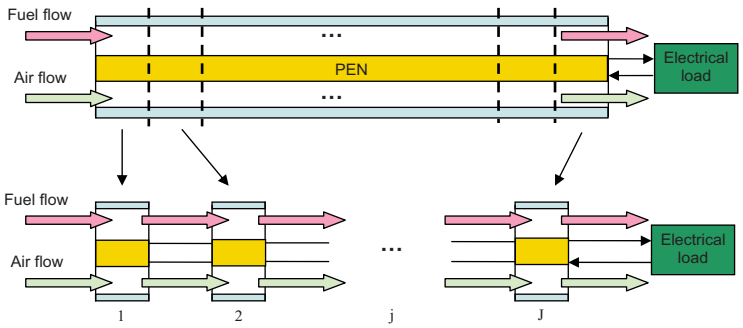

Fig. 2 Finite-volume method for modeling of co-flow planar SOFCs

Downloaded From: http://fuelcellscience.asmedigitalcollection.asme.org/ on 03/19/2013 Terms of Use: http://asme.org/terms

$$U^j = U^j_{\mathrm{OCV}} - (\eta^j_{\mathrm{ohm}} + \eta^j_{\mathrm{act}} + \eta^j_{\mathrm{con}}), \quad j = 1,2,\ldots,J \tag{1}$$

where j is the index of discretization units, as shown in Fig. 2. The last three terms in Eq. (1) are various potential losses in the jth unit. U^j_{OCV} is the open circuit voltage determined by the Nernst equation [1]. For simplicity, the superscript j will be omitted in the rest of equations given in Sec. 2.1–2.3, as the variables in those equations refer to the same discretization unit.

The activation losses η_{act} are due to the energy barriers to be overcome in order for the electrochemical reaction to occur, and can be characterized by the Butler–Volmer equation [16]. The concentration losses η_{con} reflect the overpotential due to the species diffusions between the reaction site and the bulk flow in the gas channels. The approach used in Ref. [6] is adopted here to calculate the concentration overpotentials. For completeness, the expressions for those voltage losses in Eq. (1) are given below:

$$\eta_{\mathrm{ohm}} = iAR_{\mathrm{ohm}} \tag{2}$$

$$\eta_{\mathrm{act}} = \frac{\tilde{R}T_{\mathrm{PEN}}}{F}\sinh^{-1}\left(\frac{i}{2i_{0,\mathrm{an}}}\right) + \frac{\tilde{R}T_{\mathrm{PEN}}}{F}\sinh^{-1}\left(\frac{i}{2i_{0,\mathrm{ca}}}\right) \tag{3}$$

$$\eta_{\mathrm{con}} = \frac{\tilde{R}T_{\mathrm{PEN}}}{2F}\ln\left(\frac{p_{\mathrm{H_2O},r}p_{\mathrm{H_2}}}{p_{\mathrm{H_2O}}p_{\mathrm{H_2},r}}\right) + \frac{\tilde{R}T_{\mathrm{PEN}}}{4F}\ln\left(\frac{p_{\mathrm{O_2}}}{p_{\mathrm{O_2},r}}\right) \tag{4}$$

where $i_{0,\mathrm{an}}$ and $i_{0,\mathrm{ca}}$ are the anode and cathode exchange current densities, respectively, which are functions of the temperature in PEN, as described in Ref. [6]. The subscript r represents the reaction site. Following the approach used in Ref. [6], we have

$$p_{\mathrm{H_2},r} = p_{\mathrm{H_2}} - \frac{\tilde{R}T_{\mathrm{PEN}}\tau_{\mathrm{an}}}{2FD_{\mathrm{eff,an}}}i \tag{5}$$

$$p_{\mathrm{H_2O},r} = p_{\mathrm{H_2O}} + \frac{\tilde{R}T_{\mathrm{PEN}}\tau_{\mathrm{an}}}{2FD_{\mathrm{eff,an}}}i \tag{6}$$

$$p_{\mathrm{O_2},r} = P_a - (P_a - p_{\mathrm{O_2}})\exp\left(\frac{\tilde{R}T_{\mathrm{PEN}}\tau_{\mathrm{ca}}}{4FD_{\mathrm{eff,ca}}P_a}i\right) \tag{7}$$

Therefore, the polarization relation in each discretization unit, as denoted by the following nonlinear function, can be determined in the electrochemical submodel based on the local conditions, including the PEN temperature and gas compositions:

$$U = f(i, p_{\mathrm{H_2}}, p_{\mathrm{O_2}}, p_{\mathrm{H_2O}}, P_a, T_{\mathrm{PEN}}) \tag{8}$$

It is noted that there is no state in the electrochemical submodel.

2.2 Mass Balance Submodel. The compositions and pressures of the bulk flows in the fuel and air channels are calculated in the mass balance submodel. In this submodel, each discretization unit of the cell has eight states, representing the molar concentrations of different gas species, i.e., CH_4, CO_2, CO, H_2O, H_2, and N_2 in the fuel channel, and O_2 and N_2 in the air channel.

The mass balance dynamics of the bulk flow in the fuel channel in one discretization unit can be described as follows:

$$\dot{C}_{s_f} = (N_{\mathrm{in},s_f} - N_{\mathrm{out},s_f})\frac{1}{V_f} + \sum_{k\in\{\mathrm{SR,WGS,Ox}\}} \nu_{s_f,k} r_k \frac{1}{d_f},$$
$$s_f \in \{\mathrm{CH_4,CO_2,CO,H_2O,H_2,N_2}\} \tag{9}$$

where C_{s_f} is the molar concentration of species s_f, N_{in,s_f} and N_{out,s_f} are the inlet and outlet molar flow rates of species s_f, respectively, V_f is the volume of the fuel channel in one discretization unit, $\nu_{s_f,k}$ is the stoichiometric coefficient of species s_f in reaction k, r_k is the reaction rate of reaction k, and d_f is the height of the fuel channel. All the variables refer to the same discretization unit.

Similarly, the mass balance dynamics of the bulk flow in the air channel gives

$$\dot{C}_{s_a} = (N_{\mathrm{in},s_a} - N_{\mathrm{out},s_a})\frac{1}{V_a} + \nu_{s_a,\mathrm{red}} r_{\mathrm{red}} \frac{1}{d_a}, \quad s_a \in \{\mathrm{O_2,N_2}\} \tag{10}$$

The following equations are adopted to calculate the rates of different reactions considered in the model:

$$r_{\mathrm{Ox}} = r_{\mathrm{Red}} = \frac{i}{2F} \tag{11}$$

$$r_{\mathrm{SR}} = 0.04274 p_{\mathrm{CH_4}} \exp\left(-\frac{82{,}000}{\tilde{R}T_f}\right) \tag{12}$$

$$r_{\mathrm{WGS}} = k_{\mathrm{WGS}} p_{\mathrm{CO}}\left(1 - \frac{p_{\mathrm{CO_2}}p_{\mathrm{H_2}}}{p_{\mathrm{CO}}p_{\mathrm{H_2O}}K_{\mathrm{eq,WGS}}}\right) \tag{13}$$

where k_{WGS} assumes large value, reflecting the very fast kinetics of the WGS reaction [6], and $K_{\mathrm{eq,WGS}}$ the equilibrium constant of the WGS reaction with $K_{\mathrm{eq,WGS}} \approx \exp(4276/T_f - 3.961)$ [15]. Equation (11) comes from Faraday's law. While different expressions have been proposed to represent the kinetics of the SR reaction in the SOFC, the formula described in Eq. (12) is widely used in literature [2,6,16,17].

2.3 Energy Balance Submodel. The temperature dynamics in the SOFC are calculated in this submodel. In the planar SOFC model, the cell is usually divided into several temperature layers to represent the temperature distribution along the axis perpendicular to the cell plate, and different assumptions with three to five temperature layers have been found in the models developed by different groups [2,5,6,8,12,13]. In Ref. [18], the authors compare the steady-state and dynamic simulation results of the SOFC models with different assumptions of temperature layers in the energy balance, and investigate the impacts of these assumptions on the model performance. It is found that the key dynamics of the SOFC can be preserved by assuming as few as two temperature layers–the solid structure and the air channel bulk flow. The two temperature layer assumption, as described in the following, is also adopted in this paper.

- The temperatures of the fuel flow, PEN, and interconnector are assumed equal to form one temperature layer, denoted by T_{sol}, namely, $T_f = T_{\mathrm{PEN}} = T_I = T_{\mathrm{sol}}$.
- The bulk flow in the air channel (T_a) is the other temperature layer.
- The energy accumulated in the gas inside the fuel channel is neglected.

It has been shown in Ref. [18] that combining the above two temperature layers into one will introduce significant model errors.

The heat transfer considered in the model includes the convection between the bulk flow in the air channel and its surrounding solid walls as well as the conduction in the solid structures. The governing equations for the two temperature layers, based on energy balance, are listed as follows, and the readers can refer to Ref. [18] for more detailed descriptions.

$$\dot{T}_a = \frac{1}{\sum_{s_a} c_{v,s_a} C_{s_a}}\left\{-\sum_{s_a}(h_{s_a}(T_a) - \tilde{R}T_a)\dot{C}_{s_a} + (q_{\mathrm{in},a} - q_{\mathrm{out},a})\frac{1}{l} + [k_{a,\mathrm{PEN}}(T_{\mathrm{sol}} - T_a) + k_{a,I}(T_{\mathrm{sol}} - T_a)]\frac{1}{d_a} - 0.5 r_{\mathrm{red}} h_{\mathrm{O_2}}(T_a)\frac{1}{d_a}\right\} \tag{14}$$

Downloaded From: http://fuelcellscience.asmedigitalcollection.asme.org/ on 03/19/2013 Terms of Use: http://asme.org/terms

$$\dot{T}_{\text{sol}} = \frac{1}{\rho_{\text{PEN}} c_{p,\text{PEN}} \tau_{\text{PEN}} + \rho_I c_{p,I} \tau_I} \left\{ q_{\text{cond,PEN}} \frac{\tau_{\text{PEN}}}{l} + q_{\text{cond},I} \frac{\tau_I}{l} + (q_{\text{in},f} - q_{\text{out},f}) \frac{d_f}{l} - k_{a,\text{PEN}} (T_{\text{sol}} - T_a) - k_{a,I} (T_{\text{sol}} - T_a) + 0.5 r_{\text{red}} h_{\text{O}_2}(T_a) - iU \right\} \tag{15}$$

where $h_s(T)$ is the specific enthalpy of species s at the temperature of T, q_{in} and q_{out} are the inlet and outlet enthalpy fluxes of the bulk flows in one discretization unit, respectively, $k_{a,\text{PEN}}$ and $k_{a,I}$ are the heat transfer coefficients of the air flow to the PEN and interconnector, respectively, and $q_{\text{cond,PEN}}$ and $q_{\text{cond},I}$ account for the conductive heat flux in the PEN and interconnector, respectively.

2.4 SOFC Cell Model. The model of the SOFC is then obtained by integrating the dynamic equations of all the discretization units and following the flow continuity, boundary conditions, and current distribution relations.

Based on the equipotential assumption, the following relations are imposed among the discretization units:

$$U^j = U_{\text{cell}}, \quad j = 1,2, \ldots, J \tag{16}$$

$$\sum_{j=1}^{J} I^j = \sum_{j=1}^{J} i^j A^j = I_{\text{tot}} \tag{17}$$

where the superscript j means the jth discretization unit as mentioned earlier, J is the total number of these units, U_{cell} is the operating voltage of the cell, I^j and I_{tot} are the currents drawn from the jth unit and the whole cell, respectively, and A^j is the area of the electrochemical reaction in the jth unit.

By the continuity of the gas flows, we have the following constraints for the bulk flow in the fuel channel:

$$N^j_{\text{in},s_f} = N^{j-1}_{\text{out},s_f} = u^{j-1}_{\text{out},f} C^{j-1}_{s_f} A_{c,f} \tag{18}$$

$$N^j_{\text{out},s_f} = u^j_{\text{out},f} C^j_{s_f} A_{c,f} \tag{19}$$

with $N^1_{\text{in},s_f} = N^0_{\text{out},s_f}$ being the molar flow rate of species s_f at the fuel inlet to the SOFC, and $A_{c,f}$ being the cross area of the fuel channel. $u^j_{\text{out},f}$ is the velocity of the fuel flow coming out of the jth unit, which can be determined by

$$u^j_{\text{out},f} = \frac{W^j_{\text{out},f}}{A_{c,f} \Sigma_{s_f} M_{s_f} C^j_{s_f}} \tag{20}$$

where $W^j_{\text{out},f}$ is the fuel flow rate at the outlet of the jth unit, and M_{s_f} is the molar mass of s_f.

Given the small pressure drop across the fuel cell, it is assumed that the bulk flow through the fuel channel is governed by the following linear orifice equation:

$$W^j_{\text{out},f} = \alpha_f (P^j_f - P^{j+1}_f) \tag{21}$$

where α_f is the orifice constant of the fuel channel, and P^j_f and P^{j+1}_f are the total pressures of the fuel flow in the jth and $(j+1)$th units, respectively. By the ideal gas law, we have $P^j_f = \tilde{R} T^j_f \Sigma_{s_f} C^j_{s_f}$. The boundary condition gives $P^{J+1}_f = P_0$, where P_0 is the downstream pressure of the SOFC.

For the air flow, similar equations can be derived as follows:

$$N^j_{\text{in},s_a} = N^{j-1}_{\text{out},s_a} = u^{j-1}_{\text{out},a} C^{j-1}_{s_a} A_{c,a} \tag{22}$$

$$N^j_{\text{out},s_a} = u^j_{\text{out},a} C^j_{s_a} A_{c,a} \tag{23}$$

$$u^j_{\text{out},a} = \frac{W^j_{\text{out},a}}{A_{c,a} \Sigma_{s_a} M_{s_a} C^j_{s_a}} \tag{24}$$

$$W^j_{\text{out},a} = \alpha_a (P^j_a - P^{j+1}_a) \tag{25}$$

$$P^j_a = \tilde{R} T^j_a \sum_{s_a} C^j_{s_a} \tag{26}$$

with the boundary condition of $P^{J+1}_a = P_0$ and N^1_{in,s_a} being the downstream pressure and the inlet molar flow rate of the air species fed into the fuel cell, respectively.

The enthalpy fluxes of the bulk flows in the fuel and air channels can be calculated as follows:

$$q^j_{\text{in},f} = u^{j-1}_{\text{out},f} \sum_{s_f} C^{j-1}_{s_f} h_{s_f}(T^{j-1}_f) \tag{27}$$

$$q^j_{\text{out},f} = u^j_{\text{out},f} \sum_{s_f} C^j_{s_f} h_{s_f}(T^j_f) \tag{28}$$

$$q^j_{\text{in},a} = u^{j-1}_{\text{out},a} \sum_{s_a} C^{j-1}_{s_a} h_{s_a}(T^{j-1}_a) \tag{29}$$

$$q^j_{\text{out},a} = u^j_{\text{out},a} \sum_{s_a} C^j_{s_a} h_{s_a}(T^j_a) \tag{30}$$

with $q^1_{\text{in},f}$ and $q^1_{\text{in},a}$ being the enthalpy fluxes of the fuel and air inlets supplied to the fuel cell, respectively.

By the finite volume method, the heat conduction flux in the solid structures can be calculated, for the jth unit, by

$$q^j_{\text{cond,PEN}} = \lambda_{\text{PEN}} (T^{j+1}_{\text{sol}} + T^{j-1}_{\text{sol}} - 2T^j_{\text{sol}}) \frac{1}{l^j} \tag{31}$$

$$q^j_{\text{cond},I} = \lambda_I (T^{j+1}_{\text{sol}} + T^{j-1}_{\text{sol}} - 2T^j_{\text{sol}}) \frac{1}{l^j} \tag{32}$$

where λ_{PEN} and λ_I are the thermal conductivities of the PEN and interconnector, respectively. At the adiabatic boundaries, we have $T^0_{\text{sol}} = T^1_{\text{sol}}$ and $T^{J+1}_{\text{sol}} = T^J_{\text{sol}}$.

The model represented by Eqs. (1)–(32) is developed in MATLAB/SIMULINK. The dimension and material properties given in Ref. [6] for a 0.4 m(L) × 0.1 m(W) intermediate temperature anode-supported planar SOFC are used in this paper for simulations and analyses.

The number of discretization units has significant impacts on the model accuracy and computation load. Refined discretization grids can provide more accurate spatial profiles of the variables, such as the temperature and current density distributions, and therefore lead to improved representation of the fuel cell behaviors. However, the computation time increases drastically as the number of the discretization units increases. 16 units with equal lengths are selected for the simulations in this paper, which reflects a reasonable trade-off between the model accuracy and simulation efficiency [8].

3 Low-Order SOFC Model Using Online Iterative Computation

One big challenge to use the SOFC model developed in Sec. 2 for feedback control design and analysis is attributed to its high order. For example, with the 16-unit discretization scheme, the SOFC model developed in Sec. 2 has 160 states, which is prohibitively high for most model-based control design methodologies and tools. Therefore, simplifying the planar SOFC model and making it amenable to control design tools and methodologies become an important prerequisite for subsequent control system development.

In the model developed in Sec. 2, there are ten states in each discretization unit, leading to $10J$ states in the SOFC model. Among the ten states in each unit, eight are from the mass balance

Downloaded From: http://fuelcellscience.asmedigitalcollection.asme.org/ on 03/19/2013 Terms of Use: http://asme.org/terms

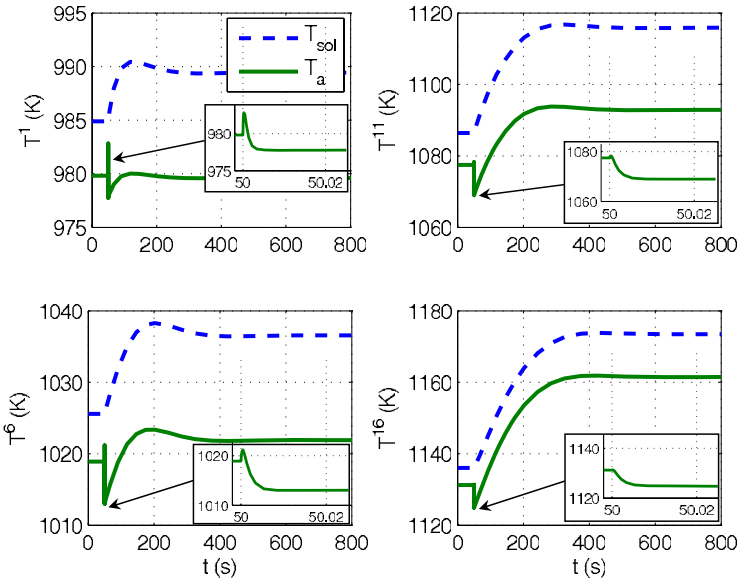

Fig. 3 Open-loop temperature response of the baseline model to step increase in current and gas supplies

dynamics and two from the energy balance dynamics. In this section, we focus on reducing the order of the SOFC model by simplifying its mass and energy balance dynamics.

3.1 Quasi-static Mass and Energy Balance in Gas Flows. Compared to the thermal dynamics in the solid structure of the SOFC, the mass and energy balance dynamics of the bulk flows in the fuel and air channels are considered much faster, due to the high speed of the gas flows and the small volumes in these channels. Since our main interest lies on the dynamics of the cell's power and temperature response, which are dictated by the thermal inertia of the solid structure in the SOFC [11], these mass and energy balance in the bulk flows can be described by quasi-static relations, i.e., the dynamics are assumed sufficiently fast to reach their steady states instantaneously [2,5,12,13]. Under this quasi-static assumption, all the governing ODEs for the gas flow dynamics, described in Eqs. (9), (10), and (14), will be replaced by the algebraic equations, thereby eliminating all the states $C^j_{s_f}$, $C^j_{s_a}$, and T^j_a, $j=1,\ldots,J$.

By setting $\dot{C}_{s_f}=0$ in Eq. (9) and with $N^j_{\text{in},s_f}=N^{j-1}_{\text{out},s_f}$, the quasi-static mass balance of gas species in the bulk flow of the fuel channel can be described as follows:

$$0 = N^{j-1}_{\text{out},\text{CH}_4} - N^j_{\text{out},\text{CH}_4} - r^j_{\text{SR}}A^j \tag{33}$$

$$0 = N^{j-1}_{\text{out},\text{CO}_2} - N^j_{\text{out},\text{CO}_2} + r^j_{\text{WGS}}A^j \tag{34}$$

$$0 = N^{j-1}_{\text{out},\text{CO}} - N^j_{\text{out},\text{CO}} + r^j_{\text{SR}}A^j - r^j_{\text{WGS}}A^j \tag{35}$$

$$0 = N^{j-1}_{\text{out},\text{H}_2\text{O}} - N^j_{\text{out},\text{H}_2\text{O}} - r^j_{\text{SR}}A^j - r^j_{\text{WGS}}A^j + r^j_{\text{Ox}}A^j \tag{36}$$

$$0 = N^{j-1}_{\text{out},\text{H}_2} - N^j_{\text{out},\text{H}_2} + 3r^j_{\text{SR}}A^j + r^j_{\text{WGS}}A^j - r^j_{\text{Ox}}A^j \tag{37}$$

$$0 = N^{j-1}_{\text{out},\text{N}_{2f}} - N^j_{\text{out},\text{N}_{2f}}, \quad j=1,\ldots,J \tag{38}$$

with $N^0_{\text{out},s_f}=N^1_{\text{in},s_f}, s_f \in \{\text{CH}_4,\text{CO}_2,\text{CO},\text{H}_2\text{O},\text{H}_2,\text{N}_{2f}\}$ being the flow rate of species in the fuel inlet to the SOFC. Note that nitrogen exists in both the fuel and the air stream: the extra subscripts, f and a, are used in Eqs. (38) and (40), respectively, to differentiate these two flow rates.

Similarly, from Eq. (10), we have the following equations for the air flow:

$$0 = N^{j-1}_{\text{out},\text{O}_2} - N^j_{\text{out},\text{O}_2} - 0.5r^j_{\text{Ox}}A^j \tag{39}$$

$$0 = N^{j-1}_{\text{out},\text{N}_{2a}} - N^j_{\text{out},\text{N}_{2a}}, \quad j=1,\ldots,J \tag{40}$$

with $N^0_{\text{out},s_a}=N^1_{\text{in},s_a}, s_a \in \{\text{O}_2,\text{N}_{2a}\}$ being the flow rate of species in the air inlet to the SOFC.

The energy balance dynamics of the bulk flow in the air channel can also be approximated using the quasi-static relationship. In Fig. 3, an illustrative example of the open-loop step response of the baseline model is shown, where the temperatures in the solid structure and air flow in the SOFC are compared. One can see that the air flow temperature exhibits dynamic behaviors at two different time scale: a very quick one (around 5 ms) immediately following the input changes in the current and the gas supplies, and a much slower one (over 300 s) tracing the temperature response in the solid structure. Since we are primarily interested in the response of the power and solid structure temperature that are defined by the slow dynamics of the energy balance in the solid structure, the energy balance dynamics in the air flow can be considered sufficiently fast to reach its steady state instantaneously. The following quasi-static energy balance equation for the air bulk flow can be obtained by setting $\dot{T}_a=0$ in Eq. (14):

$$0 = \sum_{s_a \in \{\text{O}_2,\text{N}_2\}} N^j_{\text{in},s_a}(h_{s_a}(T^{j-1}_a) - h_{s_a}(T^j_a)) + A^j(k^j_{a,\text{PEN}} + k^j_{a,I}) \times (T^j_{\text{sol}} - T^j_a), \quad j=1,\ldots,J \tag{41}$$

with T^0_a being the inlet temperature of the cathodic air flow into the fuel cell.

With the assumption of quasi-static mass and energy balance in the gas flows, the number of states in each discretization unit is reduced from 10 in the baseline model to 1 in the simplified one. The only state in each unit is T^j_{sol}, the temperature in the solid structure, which is governed by the dynamic equation given in Eq. (15).

3.2 Coupled Algebraic Equations of Quasi-static Mass Balance and Current Distribution. Although the number of states in the SOFC model is reduced substantially using the quasi-static mass and energy balance relations, the coupling between the quasi-static mass balance and current distribution leads to a large set of coupled nonlinear algebraic equations, as elaborated in the

Downloaded From: http://fuelcellscience.asmedigitalcollection.asme.org/ on 03/19/2013 Terms of Use: http://asme.org/terms

following.

While the solutions to Eqs. (38) and (40) are straightforward,

$$N^j_{\text{out},N_{2f}} = N^1_{\text{in},N_{2f}}, \quad j = 1, \ldots, J \tag{42}$$

$$N^j_{\text{out},N_{2a}} = N^1_{\text{in},N_{2a}}, \quad j = 1, \ldots, J \tag{43}$$

the equations associated with the mass balance of other species in the gas flows require the knowledge of kinetic rates of the Ox, SR, and WGS reactions. From Eq. (11), the Ox reaction rate is proportional to the local current density, which is yet to be determined.

It is noted that the partial pressures of the species are required to calculate the kinetics for SR and WGS reaction, as shown in Eqs. (12) and (13). From Eqs. (8) and (16), the partial pressures of species, such as $p^j_{\text{H}_2}$ and $p^j_{\text{O}_2}$, are also needed to determine the electrochemical polarization through the following equation:

$$U_{\text{cell}} = f(i^j, p^j_{\text{H}_2}, p^j_{\text{O}_2}, p^j_{\text{H}_2\text{O}}, P^j_a, T^j_{\text{PEN}}), \quad j = 1,2, \ldots, J \tag{44}$$

In the baseline model developed in Sec. 2, these pressure variables can be calculated from the system states (i.e., gas flow temperature and species concentrations) by directly applying the ideal gas law, and are therefore considered known in determining the mass balance dynamics and current distribution. Under the quasi-static assumption, however, those pressure variables are no longer governed by the state dynamics, but rather constrained by other algebraic relations. In this case, the species partial pressures of the fuel flow in the jth unit are calculated as follows:

$$p^j_{s_f} = X^j_{s_f} P^j_f \tag{45}$$

where $X^j_{s_f}$ is the molar fraction of species s_f in the fuel flow and can be obtained by

$$X^j_{s_f} = \frac{N^j_{\text{out},s_f}}{N^j_{\text{out},f}} \tag{46}$$

with $N^j_{\text{out},f} = \Sigma_{s_f} N^j_{\text{out},s_f}$ being the total molar flow rate of the fuel leaving the jth unit. Since the flow in the fuel channel follows the linear orifice relation described in Eq. (21), we have

$$P^j_f = P^{j+1}_f + \frac{\Sigma_{s_f} N^j_{\text{out},s_f} M_{s_f}}{\alpha_f}, \quad j = 1,2, \ldots, J \tag{47}$$

with the boundary condition of P^{J+1}_f equal to the SOFC's downstream pressure which is given.

Similarly, for the air flow, we have

$$p^j_{s_a} = X^j_{s_a} P^j_a \tag{48}$$

$$X^j_{s_a} = \frac{N^j_{\text{out},s_a}}{\Sigma_{s_a} N^j_{\text{out},s_a}} \tag{49}$$

$$P^j_a = P^{j+1}_a + \frac{\Sigma_{s_a} N^j_{\text{out},s_a} M_{s_a}}{\alpha_a}, \quad j = 1,2, \ldots, J \tag{50}$$

From Eqs. (45)–(50), all the pressure variables can be expressed as explicit functions of N^j_{out,s_f} and N^j_{out,s_a}. Therefore, the quasi-static mass balance in the gas flows and the equipotential current distribution relation result in a set of $7J+1$ coupled nonlinear algebraic equations, which consist of Eqs. (33)–(37), (39), (44), and (17), with the following $7J+1$ total unknown variables:

- N^j_{out,s_1}, $s_1 \in \{\text{CH}_4, \text{CO}_2, \text{CO}, \text{H}_2\text{O}, \text{H}_2\}$, $j = 1,2, \ldots, J$
- $N^j_{\text{out},\text{O}_2}$, $j = 1,2, \ldots, J$
- I^j, $j = 1,2, \ldots, j$
- U_{cell}

Therefore, the computational efficiency for the low-order model depends critically on the nonlinear algebraic equation solver. Without an effective algorithm, the computational advantage gained by the model order reduction effort can be easily offset by the numerical demand in solving these coupled nonlinear algebraic equations online.

3.3 Iterative Algorithm for Solving the Coupled Mass Balance and Current Distribution Algebraic Equations. A typical approach to obtain solutions to coupled nonlinear algebraic equations is to iterate on the unknown variables until all the equations are satisfied. Given the large number of unknown variables in our problem (i.e., $7J+1=113$ for $J=16$), an efficient way to find the solution is required to mitigate the computation burden involved. In this section, we first show that the quasi-static mass balance of CH_4, as described in Eq. (33), can be solved without having to know solutions to the mass balance of other gas species and current distribution. An efficient iterative computation algorithm is then proposed to solve the rest algebraic equations. The coupling relations between those unknown variables are exploited in order to reduce the number of variables that have to be iterated on. This effort leads to significant reduction in computational cost.

3.3.1 Solution to the CH_4 *Mass Balance Equation*. From Eqs. (33) and (12), we have

$$\begin{aligned} N^{j-1}_{\text{out},\text{CH}_4} &= N^j_{\text{out},\text{CH}_4} + r^j_{\text{SR}} A^j \\ &= N^j_{\text{out},\text{CH}_4} + 0.04274 p^j_{\text{CH}_4} \exp\left(-\frac{82{,}000}{\tilde{R} T^j_f}\right) A^j, \\ &\quad j = 1,2, \ldots, J \end{aligned} \tag{51}$$

It is noted that the SR reaction rate r^j_{SR} described in Eq. (12) depends only on the partial pressure of CH_4, $p^j_{\text{CH}_4}$, and the fuel flow temperature T^j_f, which is considered equal to T^j_{sol} given by Eq. (15). Under the quasi-static mass balance assumption, $p^j_{\text{CH}_4}$ can be calculated, following Eq. (45), as

$$p^j_{\text{CH}_4} = P^j_f X^j_{\text{CH}_4} \tag{52}$$

The pressure drop in the fuel flow across the planar SOFC is usually small. Therefore, we approximate P^j_f by the downstream pressure of the fuel cell P^{J+1}_f, which is known a priori. From Eq. (46), the molar fraction of CH_4 in the fuel flow of the jth unit can be computed as follows:

$$X^j_{\text{CH}_4} = \frac{N^j_{\text{out},\text{CH}_4}}{N^j_{\text{out},f}} \tag{53}$$

From the governing equations of the quasi-static mass balance given in Eqs. (33)–(38), we also have

$$\begin{aligned} N^j_{\text{out},f} &= \sum_{s_f} N^j_{\text{out},s_f} \\ &= \sum_{s_f} N^{j-1}_{\text{out},s_f} + 2 r^j_{\text{SR}} A^j \\ &= N^{j-1}_{\text{out},f} + 2(N^{j-1}_{\text{out},\text{CH}_4} - N^j_{\text{out},\text{CH}_4}), \\ &\quad j = 1,2, \ldots, J \end{aligned} \tag{54}$$

and therefore,

$$\begin{aligned} N^j_{\text{out},f} &= N^0_{\text{out},f} + 2(N^0_{\text{out},\text{CH}_4} - N^j_{\text{out},\text{CH}_4}) \\ &= N^1_{\text{in},f} + 2(N^1_{\text{in},\text{CH}_4} - N^j_{\text{out},\text{CH}_4}), \quad j = 1,2, \ldots, J \end{aligned} \tag{55}$$

By substituting Eq. (52) into Eq. (51) and considering Eqs. (53) and (55) and $P^j_f \approx P^{J+1}_f$, we have

Downloaded From: http://fuelcellscience.asmedigitalcollection.asme.org/ on 03/19/2013 Terms of Use: http://asme.org/terms

$$N^{j-1}_{\text{out},\text{CH}_4} = N^{j}_{\text{out},\text{CH}_4} + 0.04274 P_f^{J+1} \frac{N^{j}_{\text{out},\text{CH}_4}}{N^{1}_{\text{in},f} + 2(N^{1}_{\text{in},\text{CH}_4} - N^{j}_{\text{out},\text{CH}_4})} \times \exp\left(-\frac{82{,}000}{\tilde{R} T^{j}_{\text{sol}}}\right) A^j, \quad j = 1,2,\ldots,J \tag{56}$$

which defines a relation between $N^{j-1}_{\text{out},\text{CH}_4}$ and $N^{j}_{\text{out},\text{CH}_4}$. Let

$$x_j = N^{j}_{\text{out},\text{CH}_4} \tag{57}$$

$$a_j = 0.04274 P_f^{J+1} \exp\left(-\frac{82{,}000}{\tilde{R} T^{j}_{\text{sol}}}\right) A^j \tag{58}$$

$$b = N^{1}_{\text{in},f} + 2N^{1}_{\text{in},\text{CH}_4} \tag{59}$$

Eq. (56) can be rewritten as follows:

$$x_{j-1} = x_j + a_j \frac{x_j}{b - 2x_j} \tag{60}$$

from which x_j can be solved, as functions of x_{j-1}, as follows:

$$x_j^{(1)} = 0.25(2x_{j-1} + b + a_j) + 0.25\sqrt{(2x_{j-1} + b + a_j)^2 - 8bx_{j-1}} \tag{61}$$

$$x_j^{(2)} = 0.25(2x_{j-1} + b + a_j) - 0.25\sqrt{(2x_{j-1} + b + a_j)^2 - 8bx_{j-1}} \tag{62}$$

Because the reaction rate given in Eq. (12) is always nonnegative, the feasible solution to Eq. (33) should satisfy $x_j \le x_{j-1}$. Note that $b > 2N^{1}_{\text{in},\text{CH}_4} \ge 2x_{j-1}$ and $a_j > 0$, we have

$$x_j^{(1)} > 0.25(2x_{j-1} + b) \quad > x_{j-1} \tag{63}$$

rendering $x_j^{(1)}$ infeasible as a practical solution. Therefore, only $x_j^{(2)}$ given by Eq. (62) is feasible and $N^{j}_{\text{out},\text{CH}_4}$ can be solved as follows:

$$N^{j}_{\text{out},\text{CH}_4} = 0.25(2N^{j-1}_{\text{out},\text{CH}_4} + b + a_j) - 0.25\sqrt{(2N^{j-1}_{\text{out},\text{CH}_4} + b + a_j)^2 - 8bN^{j-1}_{\text{out},\text{CH}_4}}, \quad j = 1,2,\ldots,J \tag{64}$$

with the boundary condition set as the CH_4 flow rate at the fuel inlet of the SOFC, namely, $N^{0}_{\text{out},\text{CH}_4} = N^{1}_{\text{in},\text{CH}_4}$. It is most noteworthy that Eq. (64) does not require the knowledge of the rest unknown variables in the quasi-static mass balance and current distribution, and therefore, $N^{j}_{\text{out},\text{CH}_4}$, $j=1,\ldots,J$ can be solved independent of these unknown variables. The remaining unknowns, including $N^{j}_{\text{out},s_2}, s_2 \in \{\text{CO},\text{CO}_2,\text{H}_2\text{O},\text{H}_2\}$, $N^{j}_{\text{out},\text{O}_2}$, $I^j, j = 1,\ldots,J$, and U_{cell}, will be solved through the iterative computation described in the sequel.

3.3.2 Efficient Iterative Algorithm for Solving Current Distribution. Denote $I_t^j, j=1,\ldots,J$ as the total current drawn from the first j units. We now show that for $j=1,\ldots,J$, if I_t^j is given, then $N^{j}_{\text{out},s_2}, s_2 \in \{\text{CO},\text{CO}_2,\text{H}_2\text{O},\text{H}_2\}$ and $N^{j}_{\text{out},\text{O}_2}$ can be explicitly determined. One can easily verify, from Eqs. (39) and (11), that

$$N^{j}_{\text{out},\text{O}_2} = N^{1}_{\text{in},\text{O}_2} - \sum_{k=1}^{j} \frac{I^k}{4F} = N^{1}_{\text{in},\text{O}_2} - \frac{I_t^j}{4F} \tag{65}$$

For the fuel flow, after the flow rate of CH_4 being solved using Eq. (64), the WGS reaction needs to be taken into account to determine the composition of the fuel flow. As mentioned in Sec. 2, the WGS reaction in the SOFC is considered sufficiently fast to reach its equilibrium in negligible time. Therefore, the following equilibrium condition is imposed:

$$\frac{N^{j}_{\text{out},\text{CO}_2} N^{j}_{\text{out},\text{H}_2}}{N^{j}_{\text{out},\text{CO}} N^{j}_{\text{out},\text{H}_2\text{O}}} = K^{j}_{eq,\text{WGS}} \tag{66}$$

where $K^{j}_{\text{eq},\text{WGS}}$ is the equilibrium constant of the WGS reaction, with $K^{j}_{\text{eq},\text{WGS}} \approx \exp(4276/T_f^j - 3.961)$ [15].

Define

$$\phi_j = N^{1}_{\text{in},\text{CH}_4} - N^{j}_{\text{out},\text{CH}_4} \tag{67}$$

From the mass balance of the SR and Ox reactions in the first j units, ϕ_j moles of CH_4 and $(1/2F)I_t^j$ moles of H_2 react through the SR and Ox reactions in the units 1 to j, respectively. By assuming that x moles of CO react in the WGS reaction in these units, we have

$$N^{j}_{\text{out},\text{CO}_2} = N^{1}_{\text{in},\text{CO}_2} + x \tag{68}$$

$$N^{j}_{\text{out},\text{CO}} = N^{1}_{\text{in},\text{CO}} + \phi_j - x \tag{69}$$

$$N^{j}_{\text{out},\text{H}_2\text{O}} = N^{1}_{\text{in},\text{H}_2\text{O}} - \phi_j + \frac{1}{2F} I_t^j - x \tag{70}$$

$$N^{j}_{\text{out},\text{H}_2} = N^{1}_{\text{in},\text{H}_2} + 3\phi_j - \frac{1}{2F} I_t^j + x \tag{71}$$

where x needs to be determined to enforce $N^{j}_{\text{out},s_2}, s_2 \in \{\text{CO}_2,\text{CO},\text{H}_2\text{O},\text{H}_2\}$ to satisfy the equilibrium condition of Eq. (66). Given I_t^j, x can be solved by substituting Eqs. (68)–(71) in Eq. (66) and imposing the condition that $N^{j}_{\text{out},s_2} \ge 0, s_2 \in \{\text{CO}_2,\text{CO},\text{H}_2\text{O},\text{H}_2\}$. Once x is determined, molar rates for other species can be calculated using Eqs. (68)–(71).

Even though $I_t^j, j=1,\ldots,J-1$ is generally not available before the current distribution in the SOFC is determined, it is noted that for the last discretization unit, $I_t^J = I_{\text{tot}}$ is given. Thus, $N^{J}_{\text{out},\text{O}_2}$ can be determined using Eq. (65) and $N^{J}_{\text{out},s_2}, s_2 \in \{\text{CO}_2,\text{CO},\text{H}_2,\text{H}_2\}$ using Eqs. (66)–(71). The electrochemical polarization relation of $i^J - U^J$ in the last discretization unit, $U_{\text{cell}} = f(i^J, p^J_{\text{H}_2}, p^J_{\text{O}_2}, p^J_{\text{H}_2\text{O}}, P^J_a, T^J_{\text{PEN}})$, can then be determined. All the input variables to the function of f, except i^J, are now available, with the pressures calculated from N^{J}_{out,s_f}, N^{J}_{out,s_a}, P_f^{J+1}, P_a^{J+1}, and the temperature from the energy balance dynamics.

Therefore, given an initial guess of the cell's operating voltage (U_{cell}), one can calculate the current drawn from the last discretization unit (I^J) using the known polarization curve with the corresponding conditions in the last unit. By subtracting this current I^J from the total current (I_{tot}) drawn from the whole cell, we then can determine the total current for the first $J-1$ units (I_t^{J-1}). By repeating the same analysis and procedure described above and using the same voltage guess, we can proceed to calculate I^{J-1}. The process can be repeated backward along the flow direction until the first discretization unit where the equipotential current distribution conditions of Eqs. (16) and (17) are checked.

The above analysis leads to an iterative algorithm for solving the quasi-static mass balance and current distribution, given the following inputs:

- N^{1}_{in,s_f}, N^{1}_{in,s_a} fuel and air inlet conditions, respectively
- I_{tot} the total current drawn from the cell
- P_f^{J+1}, P_a^{J+1} the cell's downstream pressure
- T^{j}_{sol}, $j=1,\ldots,J$ the solid structure temperature given by the energy balance dynamics

Downloaded From: http://fuelcellscience.asmedigitalcollection.asme.org/ on 03/19/2013 Terms of Use: http://asme.org/terms

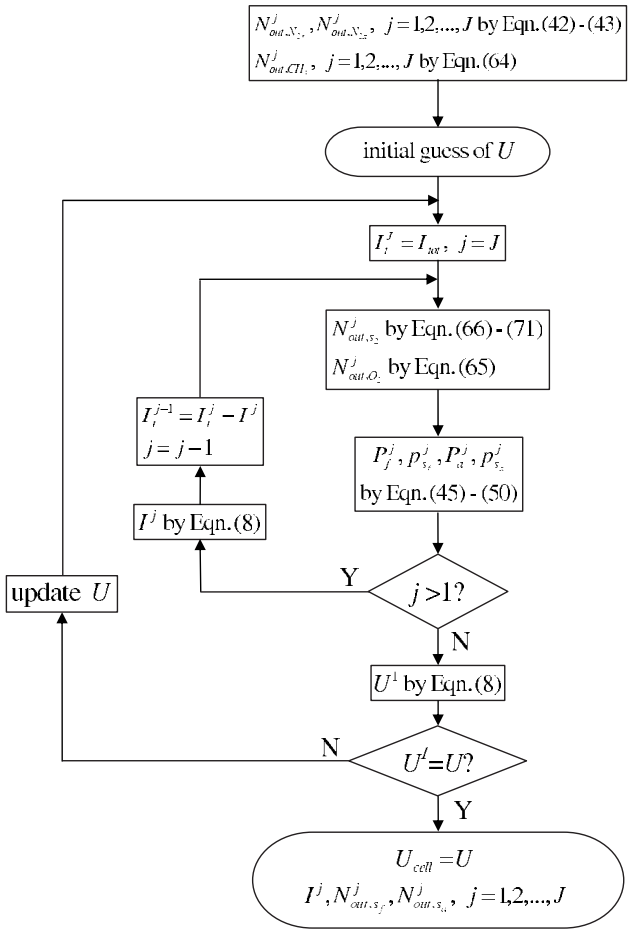

Fig. 4 Flowchart of the iterative computation for solving quasi-static mass balance and current distribution

The algorithm is outlined as follows:

1. Solve $N^j_{\text{out,CH}_4}$, $j=1,\ldots,J$ using Eq. (64) and obtain $N^j_{\text{out,N}_2f}$ and $N^j_{\text{out,N}_2a}$, $j=1,\ldots,J$ using Eqs. (42) and (43), respectively.
2. Start with an initial estimation (U) of the cell's operating voltage.
3. Initialize $j=J$ and $I_t^j=I_{\text{tot}}$.
4. Calculate N^j_{out,s_2}, $s_2 \in \{\text{CO}_2,\text{CO},\text{H}_2\text{O},\text{H}_2\}$ using Eqs. (66)–(71) and $N^j_{\text{out,O}_2}$ using Eq. (65).
5. Calculate P_f, p_{s_f}, P_a, and p_{s_a} according to Eqs. (47), (45), (50), and (48), respectively.
6. If $j>1$, calculate i^j by the polarization relation defined in Eq. (8) with $U^j=U$, let $I_t^{j-1}=I_t^j-i^jA^j$ and $j=j-1$ and go to 4. Otherwise, go to 7
7. Let $I^1=I_t^1$ and thus $i^1=I^1/A^1$. Calculate U^1 based on the polarization relation defined in Eq. (8) for given i^1.
8. If $|U^1-U|>\varepsilon$, where ε is the specified tolerance, update the estimation of U using bisection algorithm and go to 3. Otherwise, let $U_{\text{cell}}=U$ and save the results of N^j_{out,s_f}, N^j_{out,s_a} and $I^j, j=1,\ldots,J$.

The algorithm proposed here is also summarized by a flowchart shown in Fig. 4. With this algorithm, one needs to iterate only on one variable, the cell voltage, to solve the $7J+1$ coupled nonlinear algebraic equations resulting from the quasi-static mass balance and current distribution.

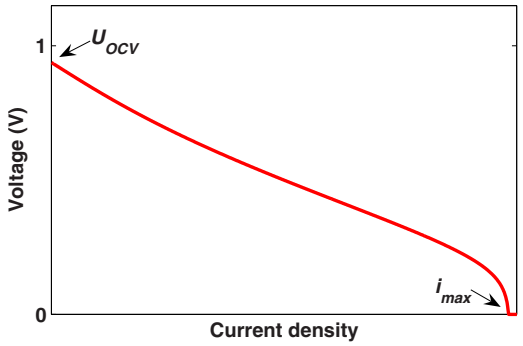

Fig. 5 Typical polarization curve in SOFC

An issue that naturally arises for the iterative algorithm given above is its convergence. To analyze the convergence, we define

$$\Delta_U = U^1(U) - U \tag{72}$$

where $U^1(U)$ is the result derived in Step 7 for a given U. Note that $\Delta_U<0$ if $U>\max_j U^j_{\text{OCV}}$ and $\Delta_U\geqslant 0$ if $U=0$, one can conclude that there must be at least one root for $\Delta_U=0$ in the interval $U\in[0,\max_j U^j_{\text{OCV}}]$ (assuming $U^1(U)$ is continuous with respect to U). The bisection approach used in our algorithm can guarantee that the solution will converge to one root [19]. More practically, there should be at least one solution within $U\in[0,\min_j U^j_{\text{OCV}}]$ at the normal operation conditions.

In fact, the solution is unique due to the monotonicity of Δ_U. Figure 5 shows a typical polarization curve defined by Eq. (8), which is monotonically decreasing in $i\in[0,i_{\max}]$. When the voltage estimation U in the iteration increases, i^J decreases and consequently I_t^{J-1} increases. From Eqs. (70) and (71) and the WGS equilibrium, $N^{J-1}_{\text{out,H}_2\text{O}}$ increases and $N^{J-1}_{\text{out,H}_2}$ decreases, resulting in a decrease in the open circuit voltage (U^{J-1}_{OCV}) and an increase in the concentration loss (η^{J-1}_{con}). Thus, the polarization curve for the $(J-1)$th discretezation unit is shifted downward. By combining with the increased U, i^{J-1} also decreases and I_t^{J-2} increases. By applying the same argument, we have $i^1=I_t^1$ increases. This effect, together with the downward shifted polarization curve in the first discretization unit, leads to a decrease in U^1 and consequently Δ_U. Therefore, Δ_U monotonically decreases in $U\in[0,\min_j U^j_{\text{OCV}}]$ as U increases, and the uniqueness of the solution is assured.

3.4 Solving Quasi-static Energy Balance Equation in Air Flow. It is noted that using the quasi-static energy balance in the air flow does not introduce any new unknown variables to the iterative algorithm proposed in Sec. 3.3, because the temperature of the air flow is not explicitly involved in the algebraic governing equations for the quasi-static mass balance and current distribution. Therefore, the solution to Eq. (41) can be pursued after the equations associated with the quasi-static mass balance and current distribution have been solved following the procedure described in Sec. 3.3.

Since the temperature change between the inlet and the outlet of the air flow in one discretization unit is limited, the first term on the right hand side of Eq. (41) can be approximated as follows:

$$\sum_{s_a} N^j_{\text{in},s_a}(h_{s_a}(T_a^{j-1}) - h_{s_a}(T_a^j)) = \sum_{s_a} N^j_{\text{in},s_a} c_{p,s_a}(T_a^{j-1})(T_a^{j-1} - T_a^j) \tag{73}$$

For the second term on the right hand side of Eq. (41), we assume that the heat transfer coefficients between the air flow and its surrounding solid walls can be approximated by constants. This is in general valid given the facts that (a) the air flow composition does not vary significantly along the air channel due to the high air excess ratio (typically above 5), and (b) the thermal conduc-

Downloaded From: http://fuelcellscience.asmedigitalcollection.asme.org/ on 03/19/2013 Terms of Use: http://asme.org/terms

tivities of O_2 and N_2 have relatively low sensitivities to the temperature in the typical SOFC operating range ($600-1000\,^{\circ}C$). The heat transfer coefficient based on the dry air at the temperature of 1073 K, denoted by $\bar{k}_a$, is used here to approximate $k^j_{a,\mathrm{PEN}}$ and $k^j_{a,I}$ in the model.

With the above approximations, Eq. (41) is simplified as follows:

$$T^j_a = T^{j-1}_a + \frac{2A^j\bar{k}_a(T^j_{\mathrm{sol}} - T^{j-1}_a)}{\Sigma_{s_a} N^j_{\mathrm{in},s_a} c_{p,s_a}(T^{j-1}_a) + 2A^j\bar{k}_a}, \quad j = 1,2,\ldots,J \quad (74)$$

where T^j_{sol} is calculated by the energy balance dynamics in Eq. (15) and $N^j_{\mathrm{in},s_a} = N^{j-1}_{\mathrm{out},s_a}$ are solved by the iterative algorithm delineated in Sec. 3.3. The boundary conditions of T^0_a and N^0_{in,s_a} are specified by the inlet condition of the air flow fed into the SOFC.

In summary, the procedure for updating the states and solving all variables involved in describing the SOFC operation is outlined as follows, given the initial operation condition N^1_{in,s_f}, N^1_{in,s_a}, I_{tot}, P^{J+1}_f, P^{J+1}_a, $T^j_{\mathrm{sol}}, j=1,\ldots,J$ at time t:

1. Solve $N^j_{\mathrm{out,CH_4}}$, $N^j_{\mathrm{out},N_2 f}$, and $N^j_{\mathrm{out},N_2 a}$, $j=1,\ldots,J$ using Eqs. (64), (42), and (43), respectively.
2. Solve $N^j_{\mathrm{out},s_2}, s_2 \in \{CO_2, CO, H_2O, H_2\}$, $N^j_{O_2}$, I^j, $j=1,\ldots,J$ and U_{cell} using the iterative algorithm proposed in Sec. 3.3.2.
3. Solve T^j_a, $j=1,\ldots,J$ using Eq. (74).
4. $t \to t+\Delta t$, update T^j_{sol}, $j=1,\ldots,J$, using the dynamic governing equation given in Eq. (15), and other operating conditions of N^1_{in,s_a}, I_{tot}, P^{J+1}_f, and P^{J+1}_a. Go to 1 to solve the quasi-static mass and energy balance and current distribution for time $t+\Delta t$.

4 Comparison of Simulation Results

For a 16-unit discretization grid, the approach proposed in Sec. 3 reduces the number of the states from 160 in the baseline model down to 16 in the simplified one. In this section, the low-order model is compared to the baseline model through simulations to evaluate the validity of the model reduction approach and the associated assumptions made in Sec. 3.

Two SOFC system configurations are considered when comparing the baseline and low-order model: one uses the fuel reformed by the CPOX technology and another assumes the SR processor. These different fuel reforming methods result in different compositions in the inlet fuel flow to the SOFC, which may have impacts on the validity of the low-order model. The operating parameters listed in Table 2 are adopted for simulations. The composition of the fuel inlet to the SOFC is also given in Table 2. The molar fraction of CH_4 in the reformate in Case 1 is 1.23%, while it is 23.5% in Case 2 due to the low prereforming ratio. For each case, the models are evaluated at both low ($i=4000\ \mathrm{A/m^2}$) and high ($i=8000\ \mathrm{A/m^2}$) loads to cover the expected operating range of the SOFC.

Steady-state responses of the low-order model and the baseline model are compared in Fig. 6, where the spacial distributions of current density, temperature, and temperature gradient in the SOFC are compared. One can see good match between these two models in both cases. For example, from Fig. 6, the location of the maximum temperature gradient in the solid structure predicted using the low-order model is the same as the baseline model, while the difference in the value of the maximum temperature gradient is less than 3% in both cases. The low-order model exhibits even smaller error in the response of cell voltage and temperature. The different inlet composition, resulting from the CPOX and SR fuel processing methods, does not have significant influence on the accuracy of the simplified model.

Table 2 Operating parameters of SOFC system

	Case 1	Case 2
Fuel processing method	CPOX	SR
Average current density ($\mathrm{A/m^2}$)	Low load: 4000 High load: 8000	
Fuel utilization	85%	
Fuel inlet temperature (K)	973	
Oxygen-to-carbon ratio	0.6	—
Steam-to-carbon ratio	—	2
Prereforming ratio	—	0.2
Reformate composition (%, molar fraction)		
CH_4	1.23	23.5
CO_2	1.71	4.55
CO	16.54	1.35
H_2O	3.42	48.4
H_2	33.1	22.2
N_2	44	0
Air excess ratio	8	
Air inlet temperature (K)	973	

The open-loop dynamic responses of the low-order model and the baseline model are also compared in Fig. 7. The parameters given in Table 2 are adopted as the operating setpoints to determine the gas inlets, such as composition, flow rate, and temperature, at low and high current loads. The current steps up from low load ($4000\ \mathrm{A/m^2}$) to high load ($8000\ \mathrm{A/m^2}$) at 100 s and steps down at 2100 s, and the gas supplies to the SOFC step up or down following the change of the current without any feedback control. It can be seen that the dynamic characteristics in the response of the low-order model are very close to the baseline model in both cases. Especially for the cell voltage, hardly any noticeable difference can be seen from Fig. 7. Similar to the steady-state results, the different fuel composition in Cases 1 and 2 has no significant impact on the model accuracy.

In Table 3, computation efficiencies of the low-order model and the baseline model are compared. The number of states in the SOFC model is calculated based on a 16-unit discretization grid. The CPU time is the average of three simulations where a 8000 s response is considered. All simulations are run on a laptop with Pentium M 1.4 GHz CPU and 512 Mbyte memory. From Table 3, it can be seen that, while the low-order model dramatically reduces the total number of states from 160 to 16, the computation time is reduced more than half as well. Although the fuel inlet composition does not affect the model accuracy as mentioned above, Case 2 with the reformate from the SR processor requires more computation time, compared to Case 1, in our study.

5 Conclusions and Future Work

In this paper, a low-order model is derived using quasi-static relations to approximate the mass and energy balance dynamics in the fuel and air bulk flows in the SOFC. In order to mitigate the computational intensity, an efficient online iterative algorithm is proposed to solve the coupled nonlinear algebraic equations for the reduced-order model. Physical relations among unknown variables are explored to reduce the online computational demand. Simulation results show that the prediction of the low-order model matches that of the baseline model with sufficient accuracy for different operating conditions. While the number of the states in each discretization unit is reduced from 10 in the baseline model to 1 in the low-order model, the computation time is also reduced more than half.

The main motivation of this model reduction effort is to provide a suitable dynamic model to facilitate control design and analysis for the SOFC system. Our future work will focus on the feedback control design for the SOFC system to ensure improved transient performance and operation safety. Given the reduced complexity

Downloaded From: http://fuelcellscience.asmedigitalcollection.asme.org/ on 03/19/2013 Terms of Use: http://asme.org/terms

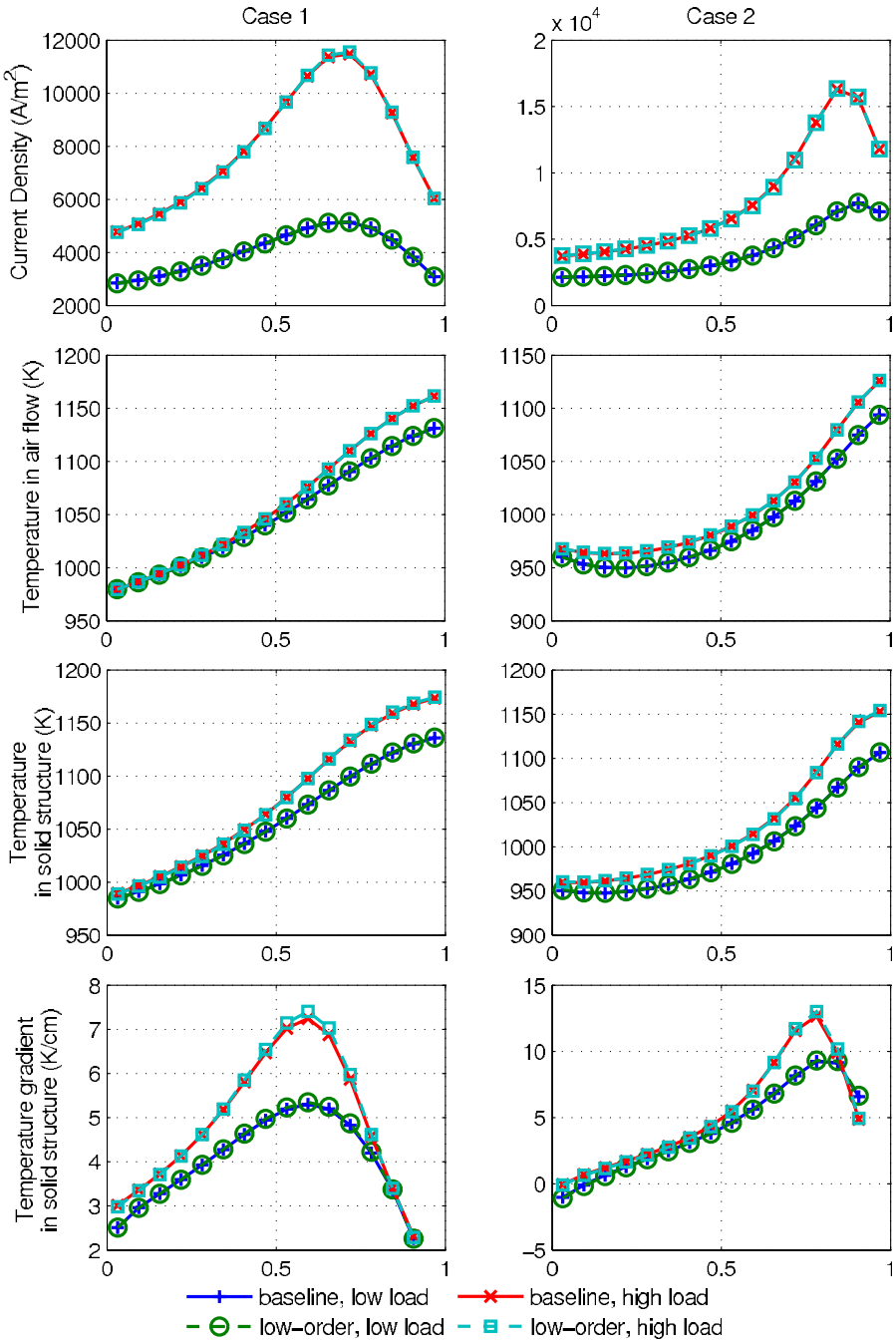

Fig. 6 Steady-state response comparison of the low-order model and the baseline model: Case 1, with CPOX reformer and Case 2, with SR prereformer

and computation cost, the low-order model developed in this paper will also be used in the evaluation and optimization of different configurations of SOFC systems.

Acknowledgment

This research was supported in part by the Department of Navy (through Office of Naval Research) under Grant No. N00014-06-1-0209 and in part by the Department of Army (through Scientific Service Program) under TCN-05158.

Nomenclature

A = area of the electrochemical reaction (m^2)
C_s = molar concentration of species s (mol/m^3)
D_{eff} = effective diffusion coefficient (m^2/s)
F = Faraday constant (C/mol)
I = electrical load current (A)
J = number of discretization units in the finite volume method
M_s = molar mass of species s (kg/mol)
$N_{in,s}$, $N_{out,s}$ = inlet and outlet molar rate of species s, respectively (mol/s)
P = total pressure (Pa)
$\tilde{R}$ = universal ideal gas constant (J/mol K)
T = temperature (K)
U, U_{cell} = operating voltage of unit and cell, respectively (V)
U_{OCV} = open circuit voltage (V)

Downloaded From: http://fuelcellscience.asmedigitalcollection.asme.org/ on 03/19/2013 Terms of Use: http://asme.org/terms

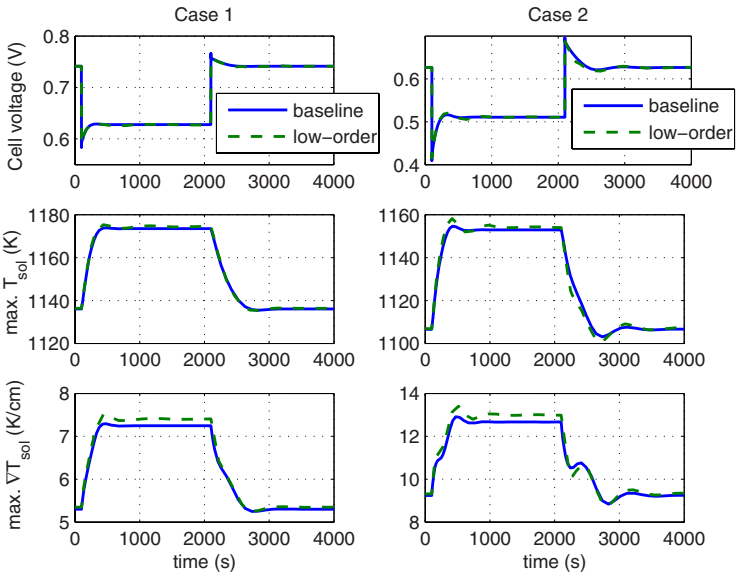

Fig. 7 Transient response comparison of the low-order model and the baseline model: Case 1, with CPOX reformer and Case 2, with SR prereformer

Table 3 Comparison of computation efficiency

Model	No. of states in each discretization unit	No. of states in SOFC model	CPU time (s)	
			Case 1	Case 2
Baseline	10	160	196	260
Low order	1	16	73	109

W_{out} = outlet mass flow rate (kg/s)
X_s = molar fraction of species s
c_p = heat capacity of solid layers (J/K kg)
$c_{v,s}$ = heat capacity of gaseous species s (J/K mol)
d = channel height (m)
$h_s(T)$ = specific enthalpy of species s at temperature of T (J/mol)
i = current density of a unit (A/m^2)
i_0 = exchange current density (A/m^2)
$k_{f,PEN}$, $k_{f,I}$, $k_{a,I}$ = heat transfer coefficients from bulk flows to solid layers ($J/K\ m^2\ s$)
l = length of cell unit (m)
p = partial pressure of gas species (Pa)
q_{cond} = heat conduction flux in solid layers ($J/s\ m^2$)
q_{in}, q_{out} = inlet and outlet enthalpy flux of gas flows, respectively ($J/s\ m^2$)
r_k = rate of reaction k ($mol/s\ m^2$)
u_{out} = outlet flow velocity (m/s)
α = orifice constant of gas channels (m s)
η = potential loss (V)
λ = thermal conductivity of solid layers (J/s m K)
$\nu_{s,k}$ = stoichiometric coefficient of species s in reaction k
ρ = density (kg/m^3)
τ = solid layer thickness (m)
I = interconnector

Subscripts

Ox = oxidation reaction
PEN = PEN structure
Red = reduction reaction
SR = steam reforming reaction
WGS = water gas shift reaction
a = air flow
act = activation
an = anode
ca = cathode
con = concentration
f = fuel flow
ohm = ohmic
r = reaction site
s_a = species in the air flow
s_f = species in the fuel flow
sol = solid structure in SOFC

Superscript

j = the jth unit

References

[1] Singhal, S., and Kendall, K., eds., 2004, *High Temperature Solid Oxide Fuel Cells: Fundamentals, Design and Applications*, Elsevier Science, New York.
[2] Achenbach, E., 1994, "Three-Dimensional and Time-Dependent Simulation of a Planar Solid Fuel Cell Stack," J. Power Sources, **49**, pp. 333–348.
[3] Haynes, C., 1999, "Simulation of Tubular Solid Oxide Fuel Cell Behavior for Integration Into Gas Turbine Cycles," Ph.D. thesis, Georgia Institute of Technology, Atlanta, GA.
[4] Ota, T., Koyama, M., Wen, C., Yamada, K., and Takahashi, H., 2003, "Object-Based Modeling of SOFC System: Dynamic Behavior of Micro-Tube SOFC," J. Power Sources, **118**, pp. 430–439.
[5] Petruzzi, L., Cocchi, S., and Fineschi, F., 2003, "A Global Thermo-Electrochemical Model for SOFC Systems Design and Engineering," J. Power Sources, **118**, pp. 96–107.
[6] Aguiar, P., Adjiman, C., and Brandon, N., 2004, "Anode-Supported Intermediate Temperature Direct Internal Reforming Solid Oxide Fuel Cell. I: Model-Based Steady-State Performance," J. Power Sources, **138**, pp. 120–136.
[7] Mueller, F., Brouwer, J., Jabbari, F., and Samuelsen, S., 2005, "Dynamic Simulation of an Integrated Solid Oxide Fuel Cell System Including Current-Based Fuel Flow Control," *Proceedings of Third International Conference on Fuel Cell Science, Engineering and Technology*.
[8] Xi, H., and Sun, J., 2005, "Dynamic Model of Planar Solid Oxide Fuel Cells for Steady State and Transient Performance Analysis," *Proceedings of ASME International Mechanical Engineering Congress and Exposition*.
[9] Achenbach, E., 1995, "Response of a Solid Oxide Fuel Cell to Load Change," J. Power Sources, **57**, pp. 105–109.
[10] Aguiar, P., Adjiman, C., and Brandon, N., 2005, "Anode-Supported Intermediate Temperature Direct Internal Reforming Solid Oxide Fuel Cell. II: Model-Based Dynamic Performance and Control," J. Power Sources, **147**, pp. 136–147.

Downloaded From: http://fuelcellscience.asmedigitalcollection.asme.org/ on 03/19/2013 Terms of Use: http://asme.org/terms

[11] Xi, H., and Sun, J., 2006, "Analysis and Feedback Control of Planar SOFC Systems for Fast Load Following in APU Applications," *Proceedings of ASME International Mechanical Engineering Congress and Exposition*.
[12] Braun, R., 2002, "Optimal Design and Operation of Solid Oxide Fuel Cell Systems for Small-Scale Stationary Applications," Ph.D. thesis, University of Wisconsin-Madison, Madison, WI.
[13] Gemmen, R., and Johnson, C., 2005, "Effect of Load Transients on SOFC Operation-Current Reversal on Loss of Load," J. Power Sources, **144**, pp. 152–164.
[14] Larminie, J., and Dicks, A., 2003, *Fuel Cell Systems Explained*, 2nd ed., Wiley, New York.
[15] Campanari, S., and Iora, P., 2005, "Comparison of Finite Volume SOFC Models for the Simulation of a Planar Cell Geometry," Fuel Cells, **5**(1), pp. 34–51.
[16] Selimovic, A., 2002, "Modeling of Solid Oxide Fuel Cells Applied to the Analysis of Integrated Systems With Gas Turbines," Ph.D. thesis, Lund University, Sweden.
[17] Campanari, S., and Iora, P., 2004, "Definition and Sensitivity Analysis of a Finite Volume SOFC Model for a Tubular Cell Geometry," J. Power Sources, **132**, pp. 113–126.
[18] Xi, H., and Sun, J., 2006, "Comparison of Dynamic Planar SOFC Models With Different Assumptions of Temperature Layers in Energy Balance," *Proceedings of ASME International Mechanical Engineering Congress and Exposition*.
[19] Bradie, B., 2006, *A Friendly Introduction to Numerical Analysis*, Prentice-Hall, Englewood Cliffs, NJ.

Downloaded From: http://fuelcellscience.asmedigitalcollection.asme.org/ on 03/19/2013 Terms of Use: http://asme.org/terms